Diurnal Variations of Presummer Rainfall over Southern China

ZHINA JIANG

State Key Laboratory of Severe Weather, Chinese Academy of Meteorological Sciences, Beijing, and Guangzhou Institute of Tropical and Marine Meteorology, China Meteorological Administration, Guangzhou, China

DA-LIN ZHANG

State Key Laboratory of Severe Weather, Chinese Academy of Meteorological Sciences, Beijing, China, and Department of Atmospheric and Oceanic Science, University of Maryland, College Park, College Park, Maryland

RUDI XIA AND TINGTING QIAN

State Key Laboratory of Severe Weather, Chinese Academy of Meteorological Sciences, Beijing, China

ABSTRACT

In this study, the presummer diurnal cycle of rainfall (DCR) over southern China is examined using the merged 0.1°-resolution gridded hourly rain gauge and satellite rainfall dataset and the National Centers for Environmental Prediction Final Global Analysis during April to June of 2008–2015. Results show pronounced diurnal variations in rainfall amount, frequency, and intensity over southern China, with substantially different amplitudes from southwestern to southeastern China, and from the pre- to postmonsoon-onset period. Southwestern China often encounters significant nocturnal-to-morning rainfall under the influence of enhanced nocturnal low-level southwesterly winds. Southeastern China is dominated by afternoon rainfall, as a result of surface heating, likely aided by local topographical lifting. Both the pre- and postmonsoon-onset periods exhibit two diurnal rainfall peaks: one in the early morning and the other in the late afternoon. But the latter shows the two peaks with nearly equal amplitude whereas the former displays a much larger early morning peak than that in the late afternoon. Three propagating modes accounting for the presummer DCR are found: (i) an eastward- or southeastward-propagating mode occurs mostly over southwestern China that is associated with enhanced transport of warm and moist air from tropical origin and the induced low-level convergence, (ii) a quasi-stationary mode over southeastern China appears locally in the warm sector with weak-gradient flows, and (iii) an inland-propagating mode occurs during the daytime in association with sea breezes along the southern coastal regions, especially evident throughout the postmonsoon-onset period.

1. Introduction

There has been considerable interest in studying the diurnal cycle of rainfall (DCR). The earliest comprehensive study of summer (June–August) DCR over the United States may be traced back to Kincer (1916), who paid attention to its impact on agricultural enterprises. Another significant work on this subject could be attributed to Wallace (1975), who studied the diurnal and semidiurnal cycles of thunderstorms associated with summer and winter

rainfall events in the United States. His study also discussed the relative importance of thermodynamic and dynamical processes in controlling the frequency and intensity of convective activity. Subsequently, a series of detailed studies on DCR over different regions of the United States was performed, which revealed a diversity of physical mechanisms (e.g., Landin and Bosart 1985; Dai et al. 1999; Liang et al. 2004; H. Chen et al. 2009; Yamada et al. 2012). Clearly, exploring DCR is useful for not only understanding regional rainfall mechanisms, but also facilitating verification of numerical weather prediction models.

In the present study, we attempt to understand some DCR characteristics during the early period of the growing season over southern China, which is located to the east
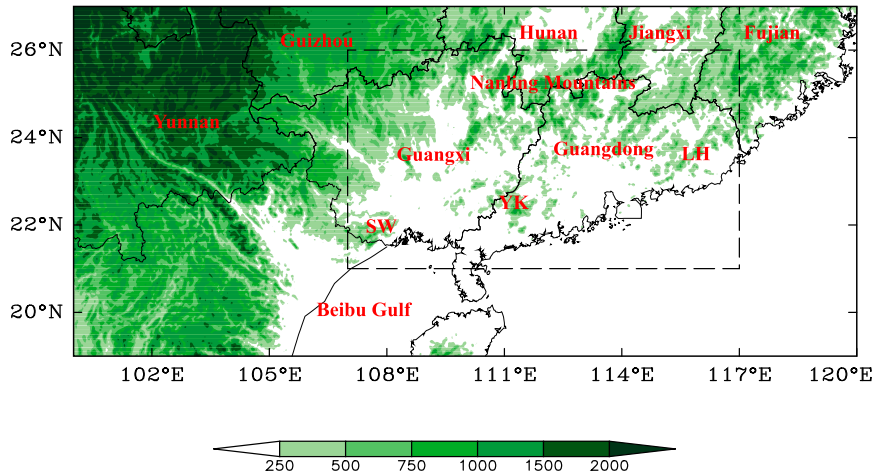

FIG. 1. Topographical (m) map of southern China. Locations of Guangdong, Guangxi, Yunnan, Guizhou, Hunan, Jiangxi, and Fujian Provinces are labeled. The solid black line represents the province border. Southern China (SC) defined in the study is the regions within the dashed boxes (21°–26°N, 107°–117°E); similarly for the dashed boxes in the subsequent figures. Letters "SW," "YK," and "LH" denotes Shiwan Mountains, Yunkai mountainous regions, and Lianhua Mountains, respectively. The Nanling Mountains are labeled. The dashed rectangular denotes our target domain.

of the Yunnan–Guizhou Plateau and the north of South China Sea (SCS) (Fig. 1). The growing-season precipitation over the region is generally affected by complex terrain, land–sea contrast, and monsoonal flows. Yu et al. (2007) was among the first to study summer DCR over contiguous China using hourly rain gauge data from 588 stations. They showed large diurnal variations of rainfall with considerable regional characteristics (e.g., it peaked in the late afternoon over southern China but around midnight over most of the Tibetan Plateau and its east periphery). Later, Zhou et al. (2008) verified the above results by comparing satellite to rain gauge observations, indicating that the diurnal phases of rainfall frequency and intensity were similar to those of rainfall amount in southern China. Li et al. (2008) explored DCR during both warm (May–September) and cold (November–March) seasons over southern China with hourly station rain gauge data. They found that cold-season rainfall peaked at midnight or early morning, due likely to the roles of the nocturnal radiative cooling at the top of continental stratus clouds in destabilizing vertical columns. In contrast, growing-season rainfall peaked in late afternoon in southeastern China due to the dominant influences of solar heating, whereas it peaked in the morning hours over southwestern China, where deep continental stratus clouds generated by the Tibetan Plateau hindered solar radiation from reaching the ground. Zheng and Chen (2011) used satellite infrared temperature of blackbody (TBB) data to explore the climatological characteristics of deep convection, denoted

by TBB ≤ -52°C, over southern China and the adjacent seas during the June–August months of 1996–2007. They found that sea–land and mountain–valley breezes accounted for the propagation of deep convection from sea to land in the afternoon and land to sea after midnight, and from mountains to plains after midnight. Chen et al. (2013) noted that the diurnal cycle of short-lived heavy rainfall events was generally consistent with that of mesoscale convective systems (MCSs) in China during the growing season. In another study, Xu and Zipser (2011) pointed out that over east of the eastern Tibetan Plateau, most of the nocturnal precipitation is in phase with MCSs and possibly contributed by long-lived MCSs evolving from late afternoon or early night convection before midsummer.

Southern China typically experiences the first rainy period from 1 April to 30 June, which is often referred to as the presummer rainy season. The presummer rainfall accounts for 40%–50% of the total annual rainfall (Huang 1986). Based on satellite observations, G. Chen et al. (2009) showed that diurnal rainfall variability was small in spring but it became pronounced during the presummer period over southeastern China. Xu et al. (2009) observed significant changes in convective intensity and mesoscale rainfall patterns, including the locations of intense rainfall and MCSs during the above transition period.

Furthermore, Chen et al. (2014) showed that convective precipitation could contribute to more than 50% of the total rainfall over the Pearl River Delta region during the presummer rainy season based on 3-yr Doppler radar data. There are two precipitation

peaks during the diurnal cycle, with the first one occurring in the early afternoon due to solar heating. Chen et al. (2015) further pointed out that the early morning peak in northern Guangdong Province was closely related to the nocturnal low-level southwesterly flow, whereas the early morning convection in Guangdong's coastal regions was triggered by the convergence between land breezes and prevailing onshore winds near the coastline.

Southern China also experiences significant changes in the prevailing winds and rainfall types after establishing monsoonal flows in mid-May (Tao and Chen 1987; Ding 1992; Ding and Chan 2005). Luo et al. (2013) noted scale differences in driving MCSs during different monsoon development stages. That is, the MCSs were less controlled by larger-scale pressure systems but more by local instability associated with solar heating during the postmonsoon and monsoon-break periods. Therefore, it is necessary to compare the spatial variability of DCR during different periods of the presummer rainy season over southern China. The purpose of this study is to illustrate the relative importance of different diurnal forcing processes in regional climate by comparing the specific contribution of DCR modes over southern China consisting mainly of Guangxi and Guangdong Provinces (see Fig. 1), during the two different periods of presummer rainy season of 2008–15. This is also one objective of the Southern China Monsoon Rainfall Experiment (SCMREX; http://scmrex.cma.gov.cn), which, as a research and development project of the World Weather Research Program of the World Meteorological Organization (WMO/WWRP), aims to advance the understanding of processes key to the heavy rain formation and to expedite the efforts to improve the prediction of heavy rainfall during the prerainy season in south China and its vicinity (Ding 1994), through field campaign, numerical weather prediction study, and physical mechanism study (Luo 2016).

The next section describes the datasets and methodology used for the present study. Section 3 shows the spatial pattern of rainfall and DCR during different periods of the presummer rainy season for the years of 2008–15. Section 4 analyzes the environmental conditions accounting for the DCR over southern China. A summary and conclusions are given in the final section.

2. Data and methodology

In this study, we use the merged rain gauge–satellite 0.1°-resolution gridded hourly precipitation dataset across China from 2008 onward (Pan et al. 2012), which were archived by the National Meteorological Information Center of the China Meteorological Administration

TABLE 1. Onset pentad of the South China Sea summer monsoon during 2008–15.

Year	2008	2009	2010	2011	2012	2013	2014	2015
Onset pentad	25	30	29	26	28	27	32	29

(CMA). This product was developed with the optimum interpolation technique by combining the CMA's hourly rain gauge network data with a satellite-retrieved precipitation product of the U.S. National Oceanic and Atmospheric Administration (NOAA), that is, the NOAA/Climate Prediction Center's morphing technique (CMORPH) dataset (Joyce et al. 2004). This dataset has been used to study the precipitation statistics of southern China by Luo et al. (2013). Large-scale meteorological conditions are analyzed using the U.S. National Centers for Environmental Prediction (NCEP) Final Global Analysis dataset, which are available on $1° \times 1°$ grids at 6-hourly intervals.

In our work, the presummer rainy season is divided into pre- and postmonsoon-onset periods, according to the onset date of the SCS summer monsoon (SCSSM; Ding and Chan 2005), which is determined by the monsoon monitoring system of the CMA's National Climate Center (NCC) (http://cmdp.ncc.cma.gov.cn/Monitoring/monsoon.htm). It is the date when (i) the 850-hPa zonal wind changes smoothly from easterly to westerly, and (ii) the 850-hPa pseudo-equivalent potential temperature (θ_e) becomes greater than 340 K over the SCS area (i.e., 10°–20°N, 110°–120°E). Table 1 lists the onset pentad of SCSSM during 2008–15. The periods before and after the onset pentad of SCSSM during the presummer rainy season are defined as the premonsoon-onset period with a total of 371 days and the postmonsoon-onset period with a total of 316 days, respectively. Note that the onset pentad of SCSSM is not included in either period.

3. Diurnal variations of presummer rainfall over southern China

Before analyzing DCR, Fig. 2 shows the mean daily rainfall (averaged by the number of total days in that period) and diurnal percentage (DP) of presummer rainfall, where DP is defined by Bao et al. (2011) as

$$\mathrm{DP} = \frac{\sum_{t=1}^{24} |r_t - \bar{r}|}{r_d}, \tag{1}$$

where r_t is the hourly rainfall amount at each hour, $\bar{r}$ is the mean hourly rainfall amount during a day, and r_d is the mean daily rainfall amount. We see from Fig. 2a
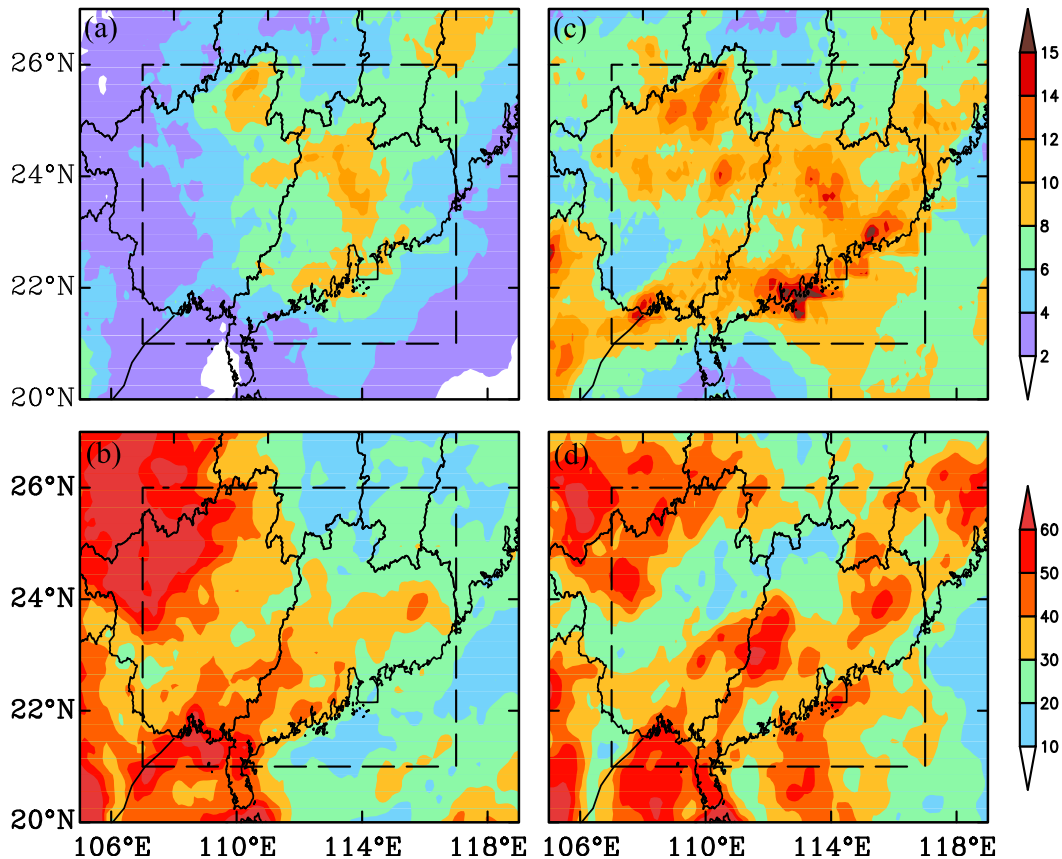
FIG. 2. Horizontal distribution of the mean daily rainfall rates (shadings, mm day^{-1}) during (a) the premonsoon-onset period and (c) the postmonsoon-onset period. The diurnal percentage (shadings, %) during (b) the premonsoon-onset period and (d) the postmonsoon-onset period.

three local maxima of the mean daily rainfall during the premonsoon-onset period, which are located over the northern portion of Guangxi Province, the north-central region, and the southern coast of Guangdong Province, respectively. These three regions continue to exhibit peak rainfall after the onset of SCSSM (Fig. 2c), and in particular, the rainfall rates over the southern coast of Guangdong Province increase rapidly (e.g., from 8 to 15 mm day^{-1}) during the postmonsoon-onset period. In addition, we can see several other rainfall centers (e.g., over the eastern coast of Guangdong, and the northeastern portion and southern coast of Guangxi). It has been speculated by Sun and Zhao (2002) that the localized rainfall maxima over the northern portion of southern China may be associated with the local trumpet-shaped topography, which facilitates the generation of low-level convergence and the subsequent development of deep convection. Chen et al. (2015) verified the topographic blocking effect on the early morning rainfall peak in northern Guangdong Province. The localized rainfall maxima along the coast of southern China coincide well with the Shiwan Mountains, Yunkai mountainous regions,

and Lianhua Mountains (see Fig. 1), suggesting again the important roles of topographical forcing in generating these rainfall features (Li et al. 2013). Figure 2b shows the highest percentage of DCR with values over 60% occurring during the premonsoon-onset period that is distributed over a southwest–northeast-oriented belt along the northwestern border of Guangxi Province, and the second highest DCR percentage that is distributed along the coastal zones (i.e., within a 100-km distance inland from the coastline) of southern China. Besides, we notice that the maximum daily rainfall centers do not always correspond to the highest DCR percentage. Of significance is that a similar pattern, but with a zone of distinct minimum in the DCR percentage between the two belts, remains during the postmonsoon-onset period (cf. Figs. 2b and 2d). These results appear to indicate (i) obvious diurnal variations of rainfall over southern China, (ii) large regional variability in DCR, and (iii) different mechanisms accounting for the rainfall generation over the different regions. They are all worth further exploring.

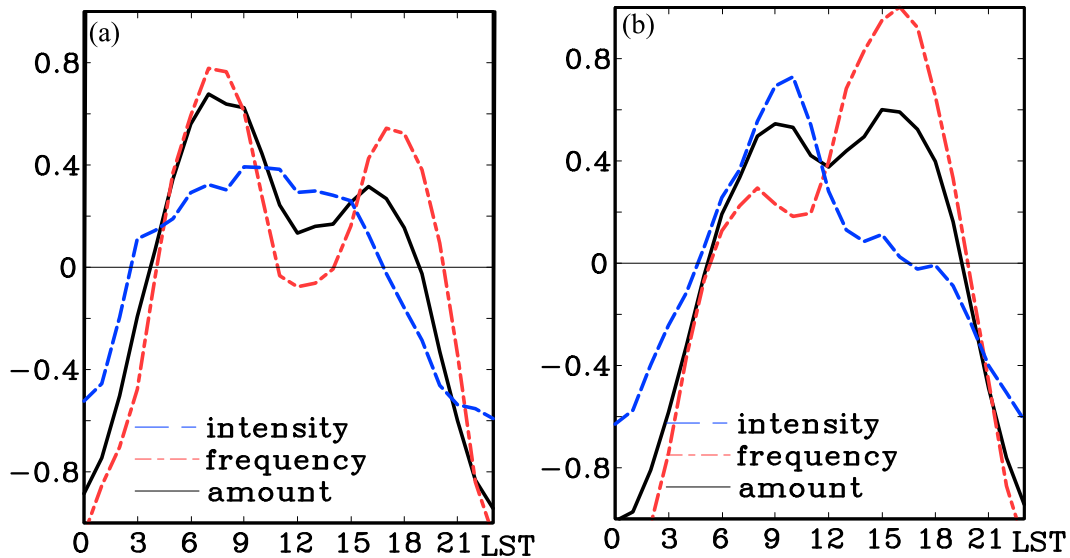Figure 3 shows the normalized (by the daily mean) DCR amount, frequency, and intensity that are averaged

FIG. 3. The normalized (by the daily mean) diurnal cycles in LST of rainfall amount, frequency, and intensity averaged over the target domain (i.e., 21°–26°N, 107°–117°E) as outlined in Fig. 1 during (a) the premonsoon-onset period and (b) the postmonsoon-onset period.

over the targeted domain (i.e., 21°–26°N, 107°–117°E; Fig. 1) in local standard time (LST). Note that southern China, which we focus on, includes two time zones. The rainfall frequency is defined as the percentage of all hours during the presummer rainy period with measurable amount (i.e., >0.02 mm h^{-1}) for the gridded rainfall as defined in Zhou et al. (2008), and the rainfall intensity is obtained by averaging the rainfall amount over the hours it occurs. Results clearly show large diurnal variations in the rainfall amount, frequency, and intensity. Two diurnal rainfall peaks are apparent: one in the morning and the other in the late afternoon. During the premonsoon-onset period (Fig. 3a), the morning peaks are stronger than the late afternoon peaks in amount and frequency, whereas, the intensity shows only one peak in the late morning. The peak rainfall is contributed by both the increased rain frequency and diurnally varying intense rain rates. In contrast, during the postmonsoon-onset period (Fig. 3b), the two rainfall amount peaks are almost equal. However, the rainfall intensity peaks in the morning, while the late afternoon rainfall frequency peak is much higher than the morning peak. This implies that the late afternoon rainfall peak may be attributed to high rainfall frequencies, whereas the morning rainfall peak may be mostly attributed to intense rainfall rates. This is consistent with the finding of Luo et al. (2013) that deep convection is more readily triggered during afternoon hours as a result of surface heating after the onset of summer monsoon.

Given the pronounced diurnal rainfall variations over southern China, Figs. 4 and 5 present the diurnal cycle of the normalized hourly rainfall deviations from the daily

rainfall mean at 3-hourly intervals during the pre- and postmonsoon-onset periods, respectively. One can see very well signals in the formation and propagation of rainfall systems across southern China. Specifically, during the premonsoon-onset period, rainfall entering into the target domain near midnight is triggered mainly on the lee side of the Yunnan–Guizhou Plateau, and then they propagate eastward in a linear shape. Although Hunan and Jiangxi Provinces appear to be another source region of rainfall, it produces a small portion of total rainfall over the northern portions of Guangxi and Guangdong. At 0200 Beijing solar time (BST) (Fig. 4a), we see a well-developed rainfall belt distributed along the western portion of Guangxi Province. Ahead of the linear-shaped rainfall belt, there are scattered weak rainfall centers over central Guangxi Province, with the leading rainfall line extending from southwestern to northeastern Guangxi and southern Jiangxi. This rainfall line coincides with the orientation of the Yunkai Mountains (Fig. 1), so the associated rainfall may be forced by the orographically induced upsloping motion in the presence of warm and moist air (discussed in the next section). Note that two rainfall belts, in which the trailing one is stronger than the leading one, are clearly seen as moving across the mountains by 0500 BST (Fig. 4b). At 0800 BST (Fig. 4c), the leading rainfall belts begin to move across the border of Guangxi and Guangdong Provinces, while the northern portion of the trailing rainfall belt is no longer evident, due likely to the removal of conditional instability by the convective activity ahead, except for its southern portion consisting of rainfall bands that are less affected.
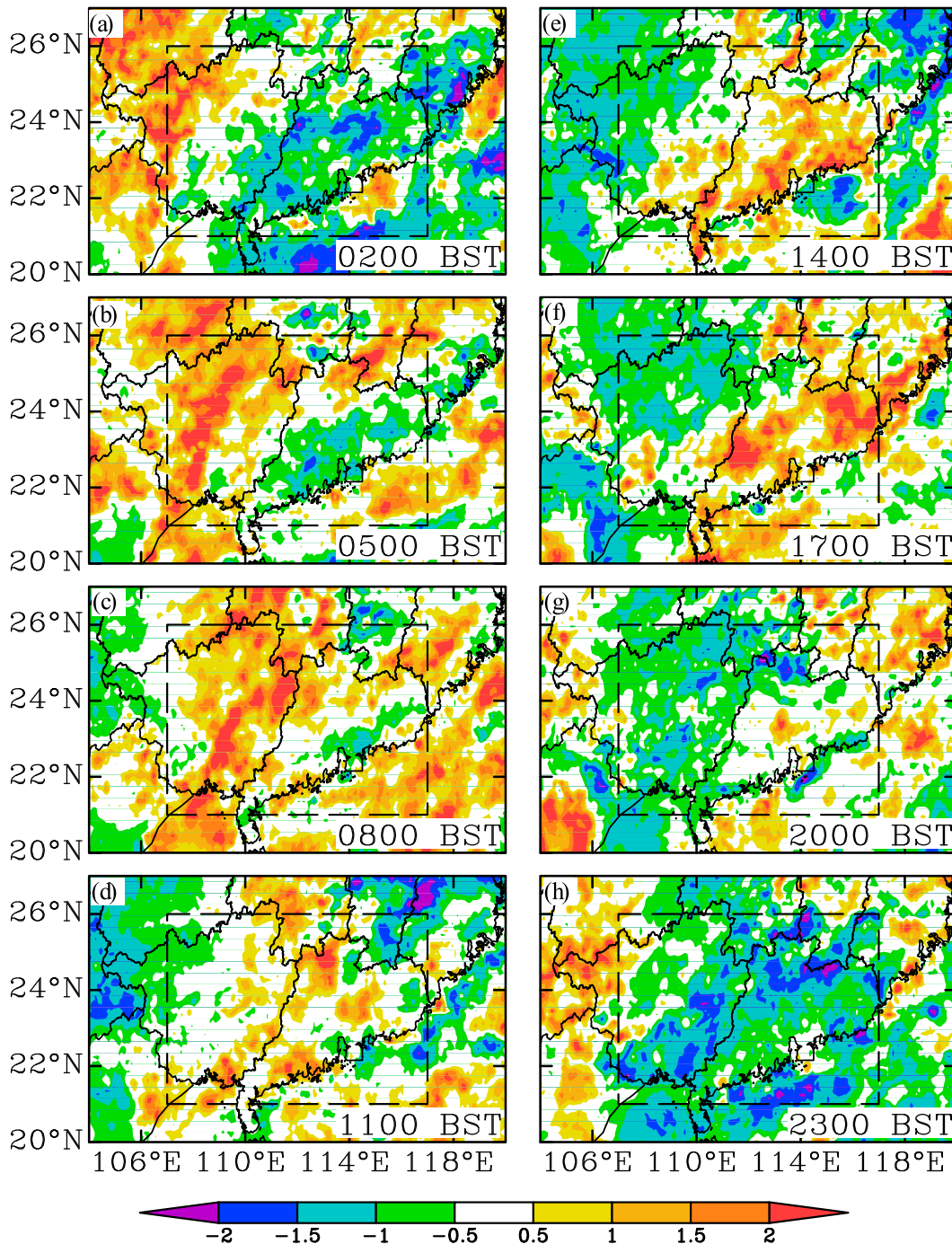
FIG. 4. Horizontal distribution of the normalized hourly rainfall deviations from the daily mean (shadings, mm h^{-1}) during the premonsoon-onset period.

An offshore rainfall belt emerging at 0200 BST is noted, and it moves outside the target domain after 1100 BST. What is more, an onshore rainfall system over the southern coast appears and spreads inward with time.

Of interest is that after the leading rainfall belt moves into Guangdong Province at 1100 BST (Fig. 4d), many rainfall systems along the rainfall belts and bands dissipate or disappear in spite of increased surface heating during the morning hours. Moreover, little significant rainfall could be seen in Guangxi Province, even during the subsequent afternoon and evening hours. More widespread and strong rainfall does not occur over
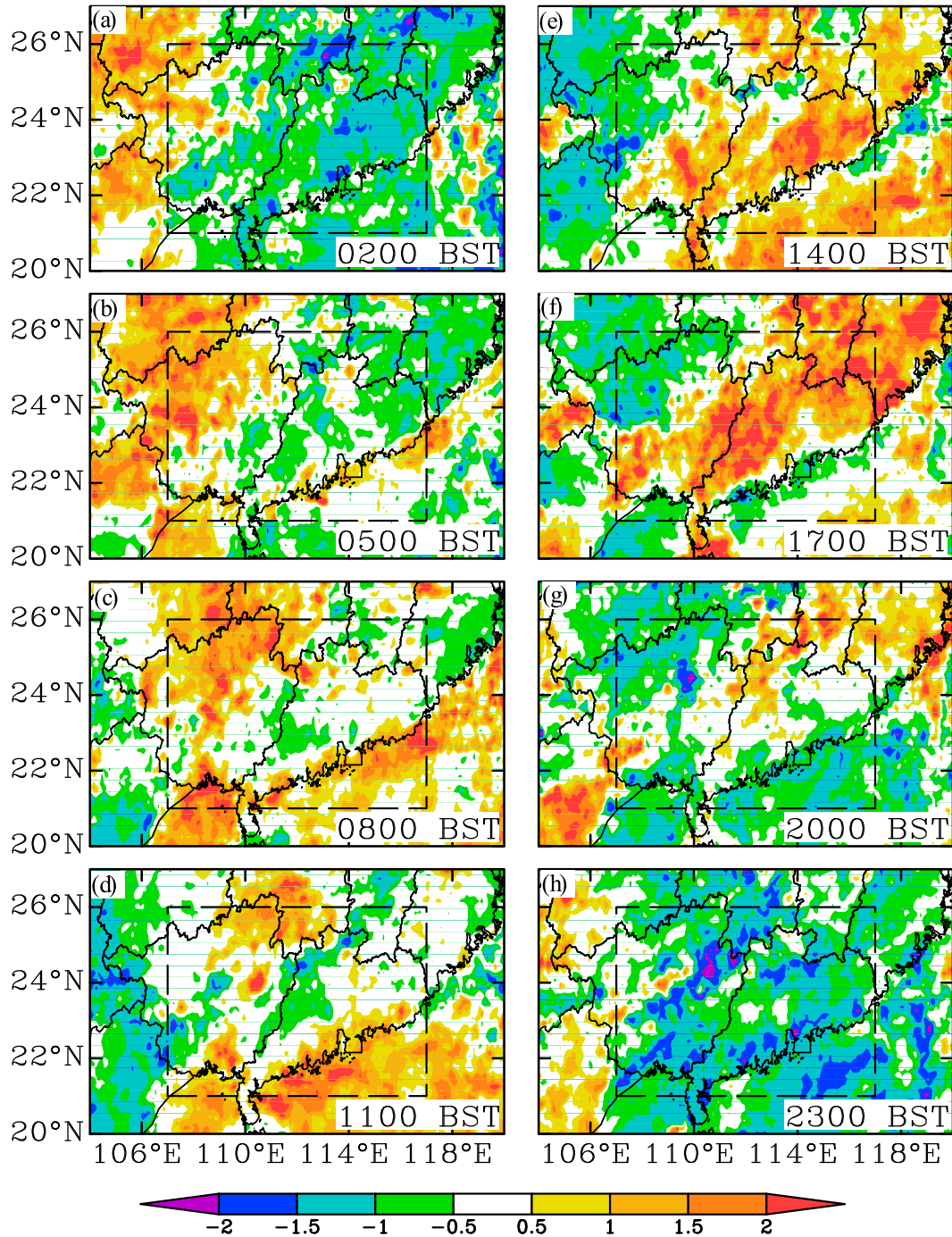
FIG. 5. As in Fig. 4, but for the postmonsoon-onset period.

Guangdong Province until 1400 BST. The distinct rainfall belt distributed through Guangdong's south- to north-central regions may be traced back to the weakened one 3 h earlier, which will be more clearly seen later (Fig. 4e). By 1700 BST (Fig. 4f), the major rainfall belt moves to Guangdong's northeastern coast and southwestern border. Subsequently, the rainfall belt

moves into the SCS at 2000 BST (Fig. 4g), and dissipates at midnight (Fig. 4h), thus completing roughly a daily life cycle. A comparison of Figs. 4 and 3a reveals clearly that the two domain-averaged rainfall peaks (i.e., around 0700 and 1600 BST) are mostly associated with the development of more active rainfall-producing systems over Guangxi and Guangdong Provinces,
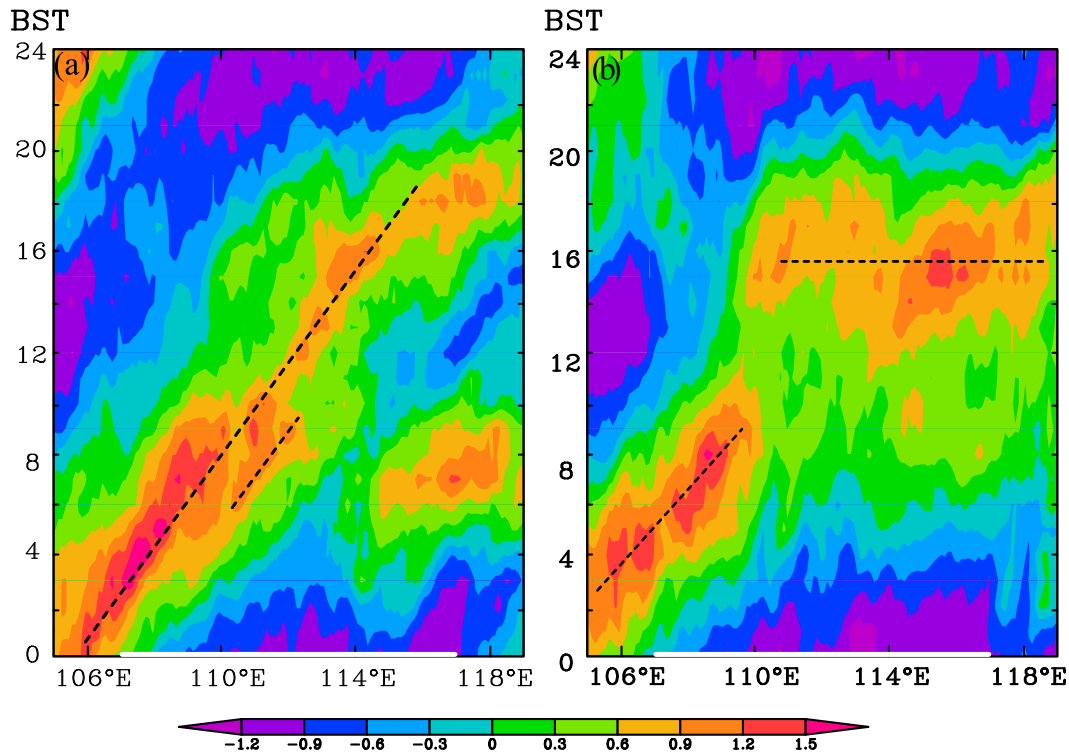
FIG. 6. Time–longitude Hovmöller diagrams of the normalized hourly rainfall deviation (shadings, mm h^{-1}) averaged from 21° to 26°N during (a) the premonsoon-onset period and (b) the postmonsoon-onset period. Dashed lines denote the axes of the peak rainfall belts. The thick white line at each bottom frame indicates the target domain of 107°–117°E.

respectively, with larger total area coverage in Guangxi Province.

During the postmonsoon-onset period, rainfalls entering the target domain in the early morning hours are mainly from the northwest, and triggered over the Guizhou Plateau, which differ from those occurring during the premonsoon-onset period (cf. Figs. 5 and 4). Although the southwestern lee side of the Yunnan–Guizhou Plateau still remains a favorable location for rainfall initiation, the rainfall systems so generated appear to shrink in size rapidly and become small sized by 1100 BST. In contrast, the rainfall from the northwest strengthens and becomes clustered with locally generated rainfall systems at 0500 BST as they propagate eastward (Fig. 5b). Meanwhile, some nocturnal rainfall systems are also generated offshore, and they strengthen as moving southeastward into the SCS. At 0800 BST (Fig. 5c), major rainfall occurs primarily over the northern half portion of Guangxi Province with a large area coverage. This is consistent with the domain-averaged rainfall peak at this time (Fig. 3b). Like the premonsoon-onset period, both the area coverage and rainfall intensity decrease during the late morning hours, with a minimum near noon (Fig. 3b). More

significant rainfall occurs on the north of the Nanling Mountains. Shortly after, however, scattered rainfall systems develop everywhere, resulting from increased surface heating, except over northwestern Guangxi Province where the planetary boundary layer must remain cold and dry after the passage of the weakened rainfall systems. In particular, numerous rainfall centers triggered at earlier times (e.g., see maps at 0500, 0800, and 1100 BST) along the southern coastal regions become strengthened and organized into an elongated rainfall band by 1100 BST (Fig. 5d). Subsequently, the coastal rainfall systems move toward inland and merges with some locally triggered rainfall systems, and by 1700 BST (Fig. 5f), a well-organized mesoscale rainfall band, with a width of about 400 km is distributed over the coastal inlands from southern Guangxi to Guangdong and Fujian Provinces. This conforms well to the peak domain-averaged rainfall in the late afternoon (Fig. 3b). The associated rainfall systems tend to be driven more by land–sea contrasts (Chen et al. 2015) and local thermodynamic conditions (e.g., conditional instability generated by surface heating) (Zhang and Fritsch 1986, 1988). The rainfall systems begin to weaken after sunset, and almost
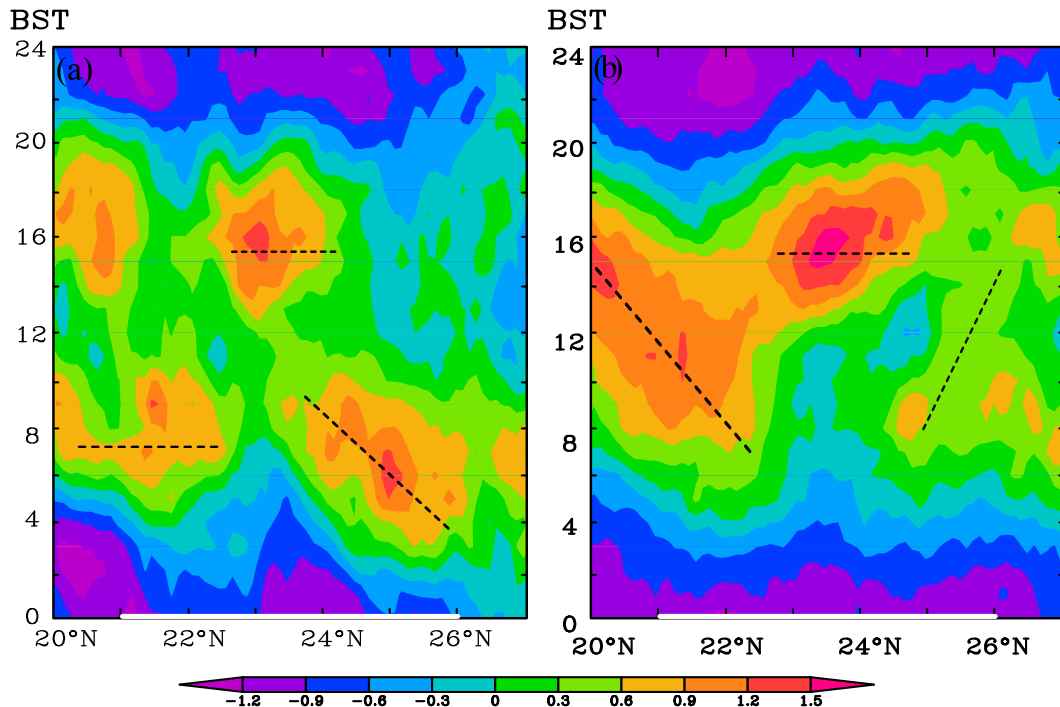
FIG. 7. As in Fig. 6 but for time–latitude Hovmöller diagrams of the normalized hourly rainfall deviation (shadings, mm h^{-1}) that are averaged between 109° and 117°E. The thick white line at each bottom frame indicates the target domain of 21°–26°N.

disappear by midnight (Fig. 5h), thus completing a daily life cycle.

To better see the zonal propagating mode of rainfall shown in Figs. 4 and 5, Fig. 6 presents the time–longitude Hovmöller diagrams of the normalized hourly rainfall deviations from the daily mean that are meridionally averaged from 21° to 26°N (i.e., the target domain width) during the two different periods. We see two distinct diurnal rainfall belts in the morning hours during the premonsoon-onset period (Fig. 6a): one enters at midnight developing on the lee side of the Yunnan–Guizhou Plateau (i.e., around 106°E), and the other is initiated shortly after midnight in Guangxi. They correspond to a major rainfall belt distributed over western Guangxi, and scattered weak rainfall centers ahead in central Guangxi. These two rainfall belts all migrate eastward at a speed of about 17 m s^{-1}, and reach their peak intensities near 0400 and 1000 BST and then they weaken prior to noon. While the major diurnal rainfall belt weakens, it appears to facilitate the subsequent initiation of widespread rainfall over Guangdong in the early afternoon hours, as the timing and location of rainfall initiation, are consistent with the eastward propagation of the weakening one. A leading diurnal rainfall belt corresponds to an intense rainfall belt along the coastline (cf. Figs. 6a and 4e–g), and then

moves offshore. Rainfall over land appears to be short lived as it disappears after sunset. In addition, we also note that there is a weak morning rainfall belt in southeast China, which corresponds to rainfall in southern Hunan Province, Jiangxi Province, and SCS shown in Figs. 4a–d.

Unlike the premonsoon-onset period, we could only see a major diurnal rainfall belt entering the target domain from the western boundary during the postmonsoon-onset period (Fig. 6b). Its eastward propagation is lagged behind that in the premonsoon-onset period, but also weakened prior to noon (cf. Figs. 6a and 6b). A major different scenario from that during the premonsoon-onset period occurs on the east of 109°E (i.e., mostly over Guangdong and eastern Guangxi Provinces). Namely, numerous diurnal rainfall belts, which look like "quasi-stationary," are locally generated in the early morning hours, and then they strengthen in the late afternoon and dissipate during the evening hours, with little evidence of zonal spatial propagation. This propagating mode accounts for a diurnal rainfall peak in the late afternoon and a minimum at midnight (Fig. 3b).

The meridional propagating mode of rainfall, shown in Figs. 4 and 5, is displayed in Fig. 7 showing the time–latitude Hovmöller diagrams of the normalized hourly rainfall deviations that are zonally averaged from

109° to 117°E during the two different periods. One can see two rainfall belts in the early morning hours over the northern and southern portions of the target domain, respectively, during the premonsoon-onset period (Fig. 7a). The southern one appears to be "weak" and "stationary," since it is more associated with the land-breeze-induced nocturnal system that moves southward out of the target domain. By comparison, the northern rainfall belt forming from outside is intense, but it begins to weaken shortly after sunrise as it moves equatorward and reaches the weakest prior to noon. Instead, one new rainfall belt is initiated along the "path" of the previously weakened one in the early afternoon over 22°–24°N, corresponding to locally generated rainfall over Guangdong Province (cf. Figs. 7a and 4e). This confirms our previous conjecture that the new rainfall belt at 1400 BST is likely initiated along cold outflow boundaries from the previously weakened rainfall [similar to the rainfall process studied in Luo et al. (2014)].

Like the premonsoon-onset period, there are also two rainfall belts occurring in the morning hours during the postmonsoon-onset period (Fig. 7b): a northern one moving polarward (i.e., toward the northeast) due to the blocking effects of the Nanling Mountains and a southern one moving equatorward associated with land breezes. Of importance is the generation of a quasi-stationary rainfall belt over the central portion in the afternoon that appears to be little influenced by the northern belt, but somewhat by the rainfall belt generated along the coastline. The presence of the quasi-stationary rain belts in both the zonally and meridionally averaged senses indicate further that most afternoon rainfall over Guangdong Province is locally generated and then dissipated in the warm sector (cf. Figs. 5e–h, 6b, and 7b).

In summary, the above analysis reveals three distinct propagating modes of DCR during the pre- and postmonsoon-onset periods: one eastward- or southeastward-propagating mode from upstream of southwestern China; and one inland-propagating mode that may be generated at daytime along the coastal regions of southern China, whose propagating mode is consistent with the deep convection found by Zheng and Chen (2011); and a quasi-stationary mode occurring locally in the afternoon likely associated with surface heating.

Before we reveal the different environmental conditions that are closely related to these DCR characteristics during the two different presummer rainy periods in the next section, two rainfall processes that show the propagation and interaction of rainfall systems are presented in Fig. 8. One rainfall process on 27 April 2008 during the premonsoon-onset period shows one isolated eastward-propagating frontal rainfall system (Figs. 8a–d). In the early morning, a rainfall system formed and entered into northern Guangxi Province at 0800 BST (Fig. 8a), and magnified at 1000 BST (Fig. 8b). It moved eastward to the border of Guangdong and Guangxi Provinces by 1500 BST (Fig. 8c) and covered most regions of western–central Guangdong Province by 1800 BST (Fig. 8d). In contrast, the other rainfall process on 1 June 2010 during the postmonsoon-onset period illustrates the propagation and interaction of multiple rainfall systems (Figs. 8e–h). At first, some scattered rainfall centers formed in Guizhou at midnight, and organized into a widespread rainfall system at 0800 BST, which covered northern Guangxi Province (Fig. 8e). With time, this rainfall system propagated eastward slowly. Simultaneously, a rainfall system along the southwestern coastline formed and strengthened (Fig. 8f). Differing from the climate-mean rainfall field, the rainfall along the coast did not move toward inland but disappeared locally. In addition, another two rainfall centers appeared over the leading of the former eastward-propagating rainfall belt at 1700 BST. By 1900 BST, these two rainfall centers over northwestern Guangdong Province interacted and finally formed one center, and at the same time the trailing strong one weakened. What is more, many scattered rainfall centers were seen to be distributed over the southern border of Guangdong and Guangxi Provinces at 1700 BST, and organized into a strong rainfall center by 1900 BST.

Clearly, the above two rainfall processes represent two types of eastward-propagating rainfall modes during the pre- and postmonsoon-onset periods, respectively. One is the frontal rainfall, which is likely associated with westerly traveling larger-scale disturbances with notable baroclinicity (e.g., surface fronts, significant upper-level differential vorticity advection, or thermal advection). The other one is an eastward-propagating rainfall but interacts later with other modes mostly driven by local thermodynamic conditions (e.g., conditional instability generated by surface heating) (Zhang and Fritsch 1986, 1988), the so-called warm-sector rainfall event (Nozumi and Arakawa 1968; Tao 1981; Zhang 1998).

4. Environmental conditions influencing the diurnal cycle of rainfall

Before examining the environmental conditions influencing the DCR presented in the preceding section, let us analyze the associated mean atmospheric circulation. For this purpose, Fig. 9 compares different large-scale flow conditions including the 850-hPa horizontal winds, its divergence and θ_e, 500-hPa geopotential heights, and 200-hPa zonal winds during the pre- and postmonsoon-onset periods. It is apparent that southern China during the premonsoon-onset period is positioned to the south of
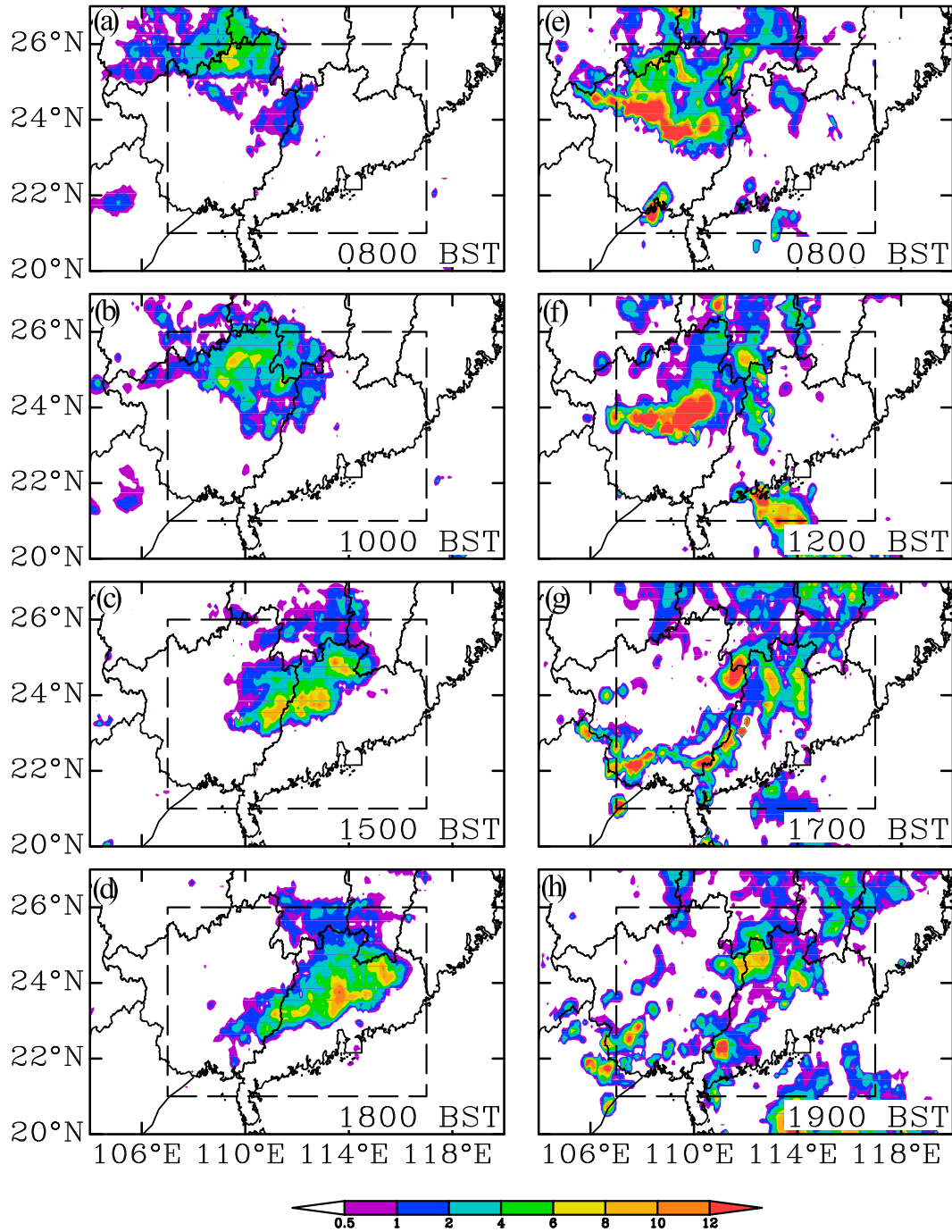
FIG. 8. Horizontal distribution of hourly rainfall (shadings, mm h^{-1}) on (a) 27 Apr 2008 and (b) 1 Jun 2010.

the entrance region of an upper-level subtropical jet exceeding 42 m s^{-1} at its core (Fig. 9a), and in the updraft branch region of a thermally direct secondary circulation. At 500 hPa, a weak-trough axis is located at the Bay of Bengal, with westerly flows extending eastward to southern China, while northwesterly flows behind a pronounced trough axis over western Pacific favor the

intrusion of colder air in the form of frontal passages. At 850 hPa (Fig. 9b), southern China is completely controlled by strong southwesterly winds associated with the western Pacific subtropical high, with a low-level southwesterly wind of 7 m s^{-1} distributed over the western half of the target domain. A large area of convergence, consistent with the secondary circulation of the upper-level
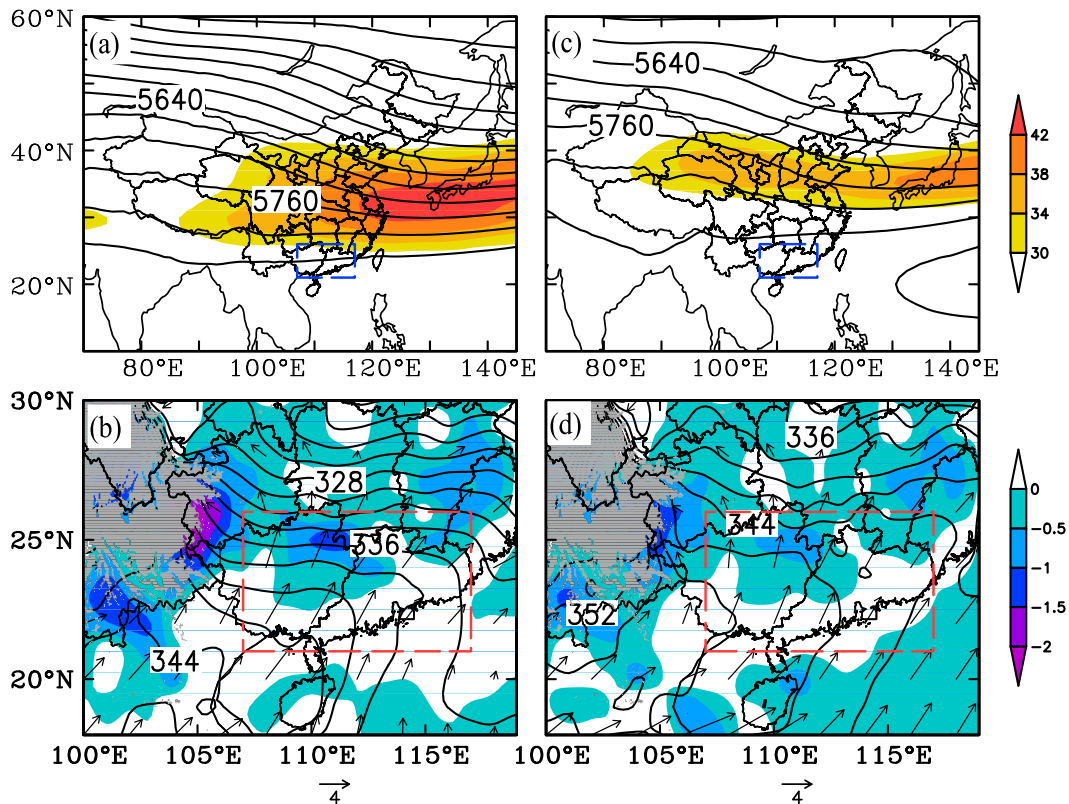
FIG. 9. Horizontal distribution of (a),(c) the 500-hPa geopotential height at 40-gpm intervals and 200-hPa zonal wind with values of greater than $30 \, \text{m s}^{-1}$ shaded. (b),(d) The 850-hPa horizontal wind vectors (m s^{-1}), divergence ($10^{-5} \, \text{s}^{-1}$) with negative values shaded, and equivalent potential temperature (θ_e, contoured at 2-K intervals) during the (a),(b) premonsoon-onset period and (c),(d) postmonsoon-onset period. Note a smaller domain size for (b),(d) than that is used for (a),(c). The gray shaded area shows the terrain elevation above 850 hPa.

jet, appears over the northern portion of southern China. Given the tropical origin of high-θ_e air of greater than 344 K, the strong southwesterly winds tends to transport the tropical high-θ_e air from the Beibu Gulf and SCS into southern China that could be easily lifted over the convergence region during its northward course. It follows that the premonsoon-onset rainfall in southern China is positively influenced by northwesterly traveling disturbances from the midlatitudes, southwesterly transport of the high-θ_e air of tropical origin, and a favorable secondary circulation associated with an upper-level jet stream.

After the onset of SCSSM (Figs. 9c,d), the upper-level subtropical jet stream core moves eastward and weakens to $38 \, \text{m s}^{-1}$, while the low-level southwesterly wind shifts to the central portion of the target domain with decreased magnitudes. However, the 500-hPa trough over the Bay of Bengal strengthens, allowing more high-θ_e air from this region than that at an earlier period to be transported to higher latitudes. Moreover, the north–south pressure gradients over southern China becomes much weaker than those occurring before as the subtropical high intensifies and extends westward beyond 140°E

(cf. Figs. 8a and 8c). Similarly, a large area of convergence appears over the northern portion of southern China, but with reduced intensity. The presence of the weak-gradient flows and weak convergence indicates less dynamical roles of large-scale flows, especially upward lifting, in conditioning regional environments for rainfall production. On the other hand, most regions of southern China are distributed with higher-θ_e air than that during the premonsoon-onset period, as also indicated by the 500-hPa height field (cf. Figs. 9b and 9d). The above results suggest that most of the postmonsoon-onset rainfall over southern China is produced in an environment with weak gradients, weak large-scale forcing, but stronger southwesterly transport of higher-θ_e air. Deep convection tends to be triggered during the afternoon hours due to surface heating, aided by local topography, and may spread into larger scales due likely to the continued energy supply and mesoscale organization (Chen et al. 2014).

With the above large-scale flow conditions in mind, we may now examine the diurnal variations of regional circulations, especially at the lower levels, over
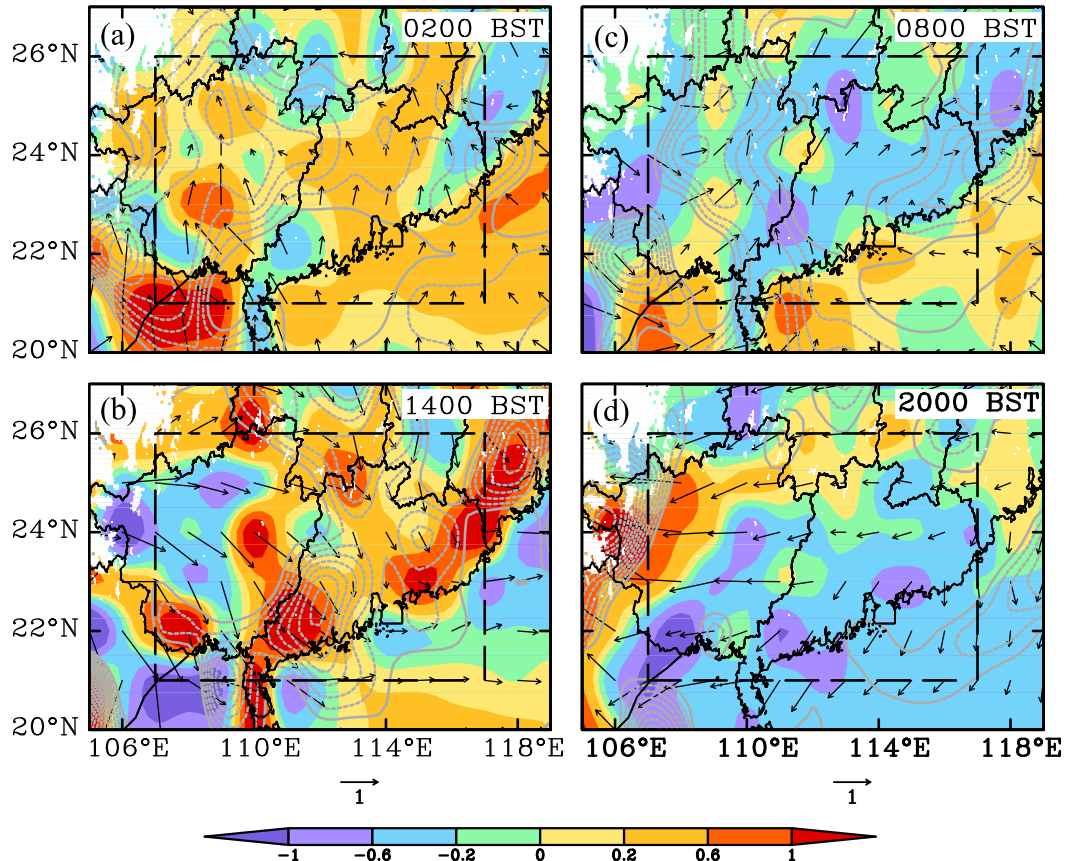
FIG. 10. Horizontal distribution of the perturbation horizontal wind vectors (m s^{-1}) and vertical motion deviations (shaded, cm s^{-1}) with respect to their daily means at 850 hPa at (a) 0200, (c) 0800, (b) 1400, and (d) 2000 BST during the premonsoon-onset period.

southern China during the two different periods. Figure 10 shows the vertical motion deviations, horizontal perturbation wind vectors, and divergence with respect to their daily means at 900 hPa, while Fig. 11 shows the west–east vertical cross sections of the meridional wind deviations and temperature advection superimposed by in-plane flow vectors, at 6-hourly intervals during the premonsoon-onset period. In general, low-level winds experience inertial oscillations (i.e., with clockwise rotation) within a diurnal cycle. At 0200 BST (Fig. 10a), the target domain is dominated by upward motion with higher magnitudes in the southwestern part and convergence in the western one-third portion with its center over northwestern part (i.e., on the lee side of the Yunnan–Guizhou Plateau), where organized nocturnal rainfall systems begin to enter the domain of interest. More importantly, the regions of stronger upward motion are distributed with more enhanced southerly flows. The southerly winds having a maximum at about 950 hPa decelerate gradually northward, indicating the enhanced convergence of tropical high-θ_e air for latent heat release

in rainfall (Figs. 10a and 11a). This strongest upward branch, along with its western downward motion, forms an anticlockwise vertical circulation over the lee of Yunnan–Guizhou Plateau (Fig. 11a). Such a favorable condition is absent over the eastern two-thirds portion of the target domain, which is consistent with the absence of significant rainfall there. The importance of the enhanced energy supply in determining the nocturnal rainfall production over southern China, mentioned above, appears to differ from that of Li et al. (2008) who believed the important contribution of inhomogeneous nocturnal radiative cooling associated with the plateau–plain contrast to the nocturnal rainfall generation on the lee side of the Tibetan Plateau. In addition, it is found that the temperature advection is strong over southwestern China below 700 hPa, which means notable baroclinicity exists over this region. This characteristic still maintains for a while though weakening with time (Fig. 11).

While pronounced rainfall in intensity and area coverage occurs over the Guangxi Province at 0800 BST (Fig. 4c), the southerly component of horizontal deviation
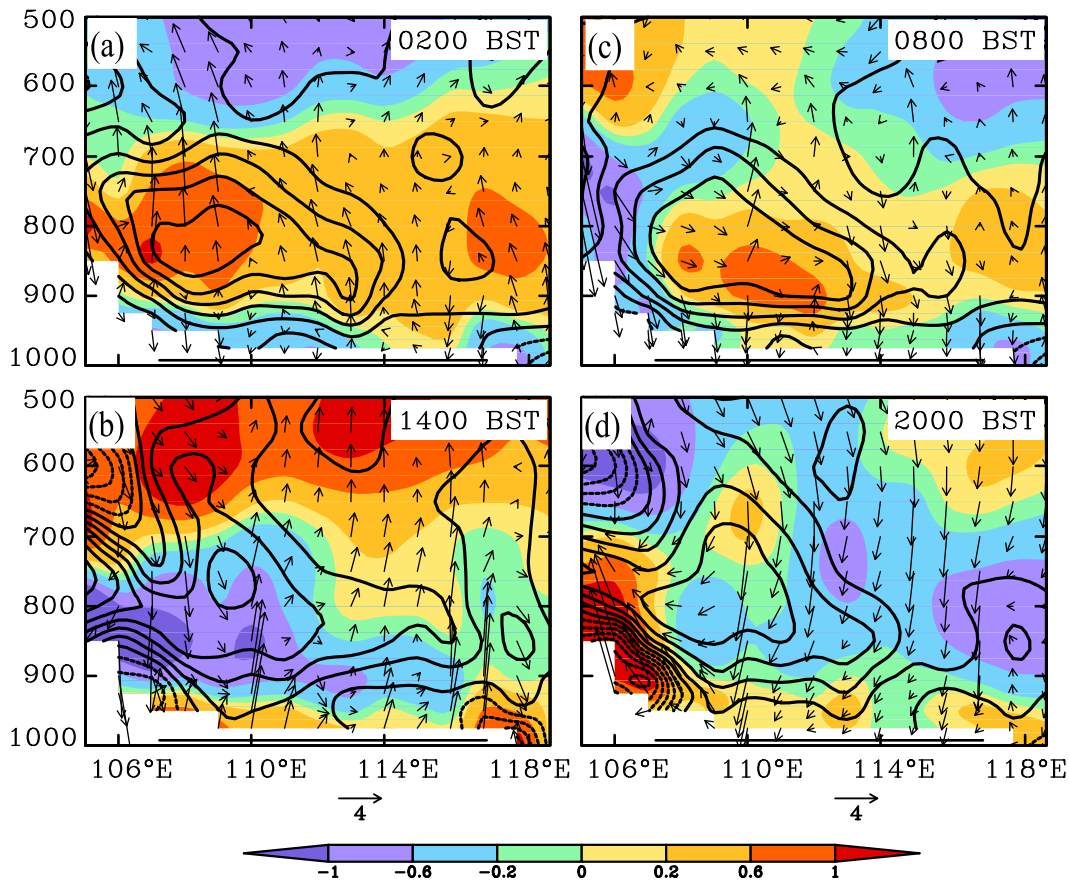
FIG. 11. Zonal-vertical cross sections of meridional velocity deviations (shaded; m s^{-1}) and temperature advection (black contoured at 1.0×10^{-5} K s^{-1} intervals) from their daily means, superimposed with in-plane flow vectors (zonal wind: m s^{-1}; vertical velocity: cm s^{-1} multiplied by 5), along 24°N at (a) 0200, (c) 0800, (b) 1400, and (d) 2000 BST during the premonsoon-onset period. The white shaded area shows the averaged terrain elevations, and the black solid lines at each bottom frame denote the target region of 107°–117°E; similarly for the rest of figures.

winds from southwestern China decreases significantly, with the maximum centers moving downward and eastward (Figs. 10c and 11c). This implies reduced supply of tropical high-θ_e air for the development of rainfall. Moreover, the corresponding anomalous upward motion decreases in both intensity and volume with strong horizontal westerly component wind. The convergent center associated with the perturbation horizontal wind also moves eastward, facilitating an eastward propagation of rainfall in the upper-level westerly mean flow. In addition, it seems that the eastern boundary of the upward motion is consistent with the orientation of topography on the border of Guangxi and Guangdong Provinces, which emphasizes the role of topographic blocking on the upward motion of high-θ_e air. These all also indicate the subsequent weakening of rainfall production, which are in agreement with those shown in Figs. 3a, 4c, and 6a. Certainly, the accelerated low-level southwesterly wind still contributes to the

early morning rainfall, which is different from the early morning rainfall in the lower Yangtze River valley in Chen et al. (2010) that is mainly related to the convergence caused by the southwesterly anomaly on its south combined with the northeasterly anomaly over its north. At 1400 BST, southwestern China is dominated by anomalous northwesterly winds while southeastern China is controlled by nearly calm westerly anomalous winds (Figs. 10b and 11b), with a further reduced supply of tropical high-θ_e air. Prevailing downward and upward motions, divergence, and convergence are distributed over Guangxi and Guangdong Provinces, respectively, coinciding well with the absence and presence of rainfall. Because of the lacking larger-scale energy supply, the widespread afternoon rainfall over Guangdong is doomed to be short lived (cf. Figs. 10b, 11b, and 4). It implies that the rainfall over southeastern China at this time is closely related to the weak environmental gradients over the region (e.g., weak temperature advection; Fig. 11b). At
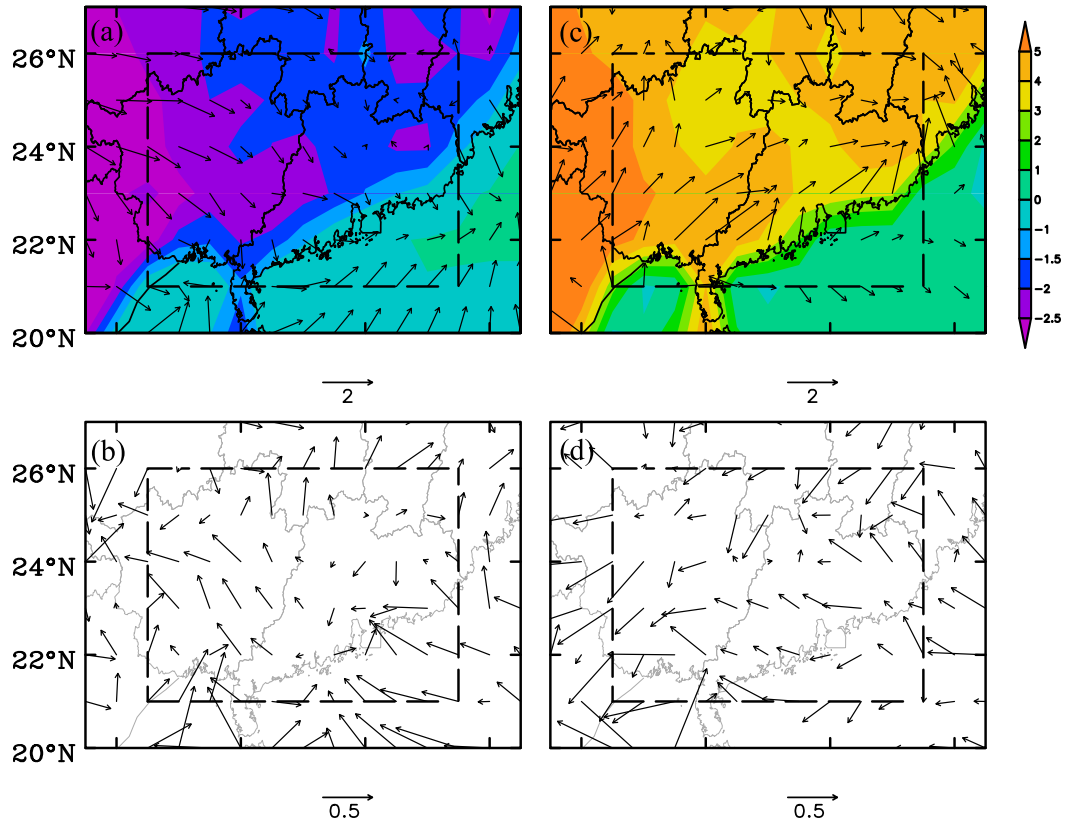
FIG. 12. The wind vector (m s^{-1}) and temperature (shaded; K) differences between (a) 0200 and 2000 BST and (c) 1400 and 0800 BST on the surface during the premonsoon-onset period. The wind vector (m s^{-1}) difference at the surface during post and premonsoon-onset period between (b) 0200 and 2000 BST and (d) 1400 and 0800 BST.

2000 BST, southern China is controlled by anomalous easterly to northeasterly winds and downward motion, even over its adjacent ocean regions, which corresponds to the diminishing rainfall production (Figs. 10d and 11d).

The diurnal variation can also be clearly illustrated in the differenced wind and temperature field in the surface layer. Between 0200 and 2000 BST during the premonsoon-onset period (Fig. 12a), the diurnal variation of temperature over land is significantly lower than that over sea, and the wind difference is mostly offshore, which indicates the development of land breeze at night. The early morning rainfall along south-coastal regions appears to be triggered by the convergence between land breezes and the prevailing onshore winds. However, the wind difference between 1400 and 0800 BST during the premonsoon-onset period is mostly onshore (Fig. 12c), induced by the temperature contrast of higher diurnal variations over land, suggesting the development of sea breezes and accounting for the propagation direction of rainfall in the afternoon. Therefore, the development of land and sea breezes at different times can explain the nocturnal rainfall initiation along

the coastline and its northeastward propagation over inland during the afternoon. This finding is consistent with Chen et al. (2015) who pointed out the role of land–sea breezes in the triggering and propagation of rainfall along the coastline over southern China. In addition, the temperature differences induced by the mountain–land contrast over southwestern China with higher temperature over its west is consistent with the downward motion over most of Guangxi Province and upward motion in Yun-Gui Plateau (Fig. 11b). Meanwhile, the temperature differences induced by the land–sea contrast over southeastern China with higher temperature over land can explain rainfall associated with the upward motion in the afternoon over Guangdong Province.

Inertial oscillations of the low-level winds can also be seen occurring during the postmonsoon-onset period (Figs. 13 and 14). At 0200 BST (Figs. 13a and 14a), the target domain is dominated by upward motion but with higher magnitudes in the northwestern portion of Guangxi Province, and by southerly to southeasterly flows but with stronger southerly component in the western portion with the maximum center around 950 hPa. The
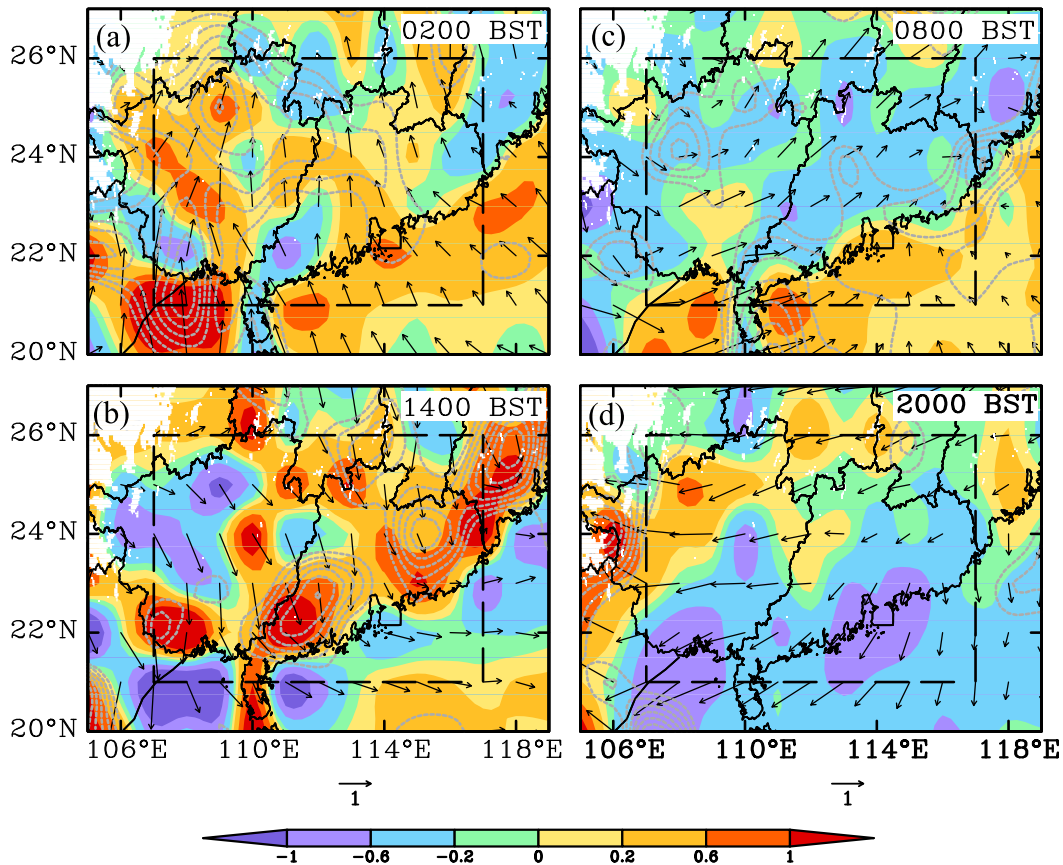
FIG. 13. As in Fig. 10, but for the postmonsoon-onset period.

convergent center is also located over its western part. They are consistent with the development of significant rainfall over the regions (Fig. 5a). Strong temperature advection can also be seen over southwestern China in the lower level, which remains until 0800 BST (Figs. 14a,c). This further illustrates that the atmosphere has the notable baroclinic characteristics over this region in the morning. Although the upward motion at 0800 BST is still present in the northwestern portion of Guangxi, the supply of tropical high-θ_e air is reduced as the southerly deviation winds have been shifted to near westerly at 850 hPa (Fig. 13c). The meridional transport concentrates between 900 and 800 hPa but with smaller amplitudes compared with that at 0200 BST (Figs. 14a and 14c). This is in agreement with the weakening rainfall as it moves southeastward during the morning hours (Figs. 5b–d). The inertial oscillations of the low-level winds further reduce the supply of tropical high-θ_e air during the rest of the diurnal cycle. It seems that whether during the pre- or postmonsoon-onset period, the accelerated southerly winds and its associated strong low-level convergence play an important contribution to the eastward- or southeastward-propagating mode mostly over southwestern China. This result is similar to

the explanation for the eastward-propagating rainfall events over central China (Chen et al. 2012), which are supported by the low-level convergence that moves from the east slope of the Tibetan Plateau to the middle reach of Yangtze River Valley, as the deviated wind vector rotates clockwise to enhance southerlies at late night and southwesterlies in the morning. And then, intense upward motion or deep convection could be only present in the afternoon (e.g., at 1400 BST) (Figs. 13b and 14b), over Guangdong Province. Without the continued favorable energy supply, little rainfall occurs over southern China after sunset (i.e., at 2000 BST) (Figs. 13d and 14d).

In addition, we could see that the wind differences over Guangdong between 0200 and 2000 BST during the postmonsoon onset are more offshore than those during the premonsoon onset (Fig. 12b). This means that the land breezes and their induced convergence along southeastern coast at night during the postmonsoon onset are stronger than those during the premonsoon onset. Thus, it is easier to trigger the midnight rainfall along the southeastern coast after summer monsoon onset. In contrast, the wind differences over Guangdong between 1400 and 0800 BST are more onshore during the
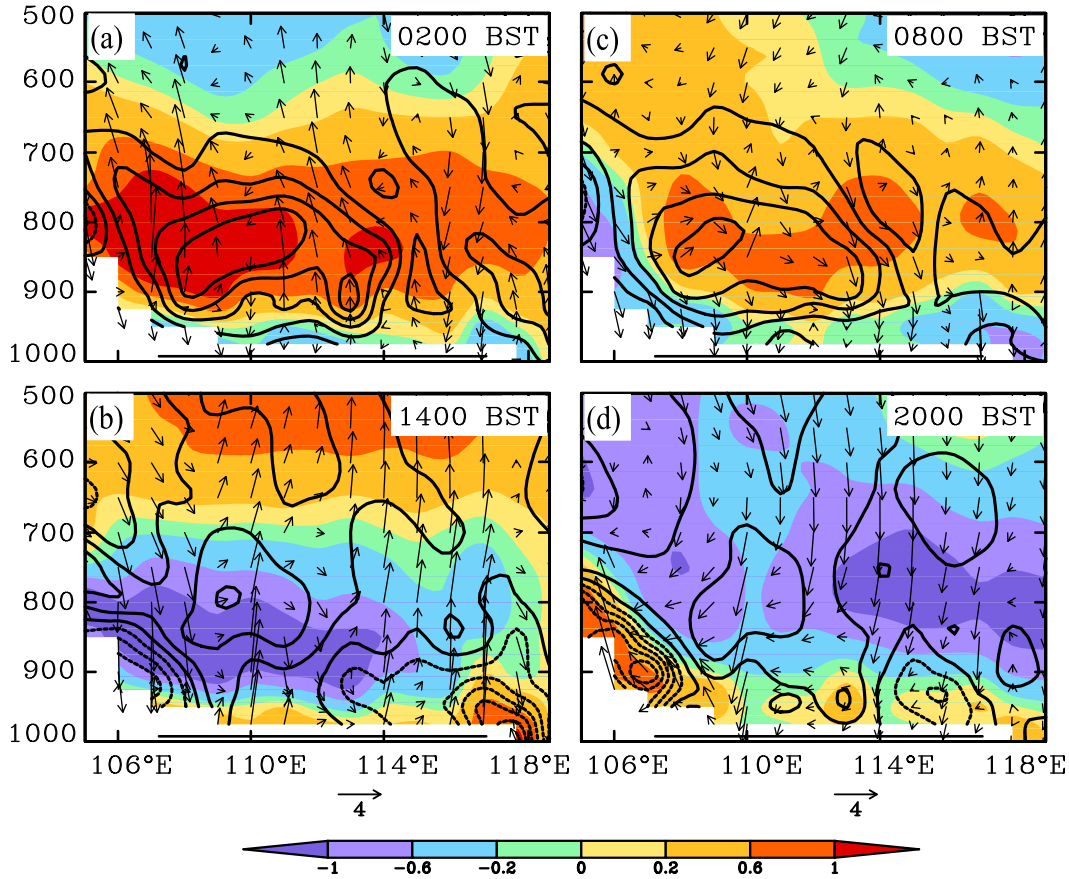
FIG. 14. As in Fig. 11, but temperature advection interval at $6.0 \times 10^{-6}\,\mathrm{K\,s^{-1}}$ for the postmonsoon-onset period.

postmonsoon onset (Fig. 12d), which is also beneficial to the farther inland propagation of rainfall in the afternoon. Therefore, the stronger offshore winds in the morning and onshore winds in the afternoon during the postmonsoon onset can explain the evident rainfall generation along the southeastern coast and more inland propagation of rainfall during the daytime.

There is also another DCR difference between the pre- and postmonsoon-onset periods over southeastern China, namely, the eastward-propagating signal is decaying while the local one is enhancing with the coming summer. The decaying propagating signal has been linked to the weaken steering westerly by comparing Figs. 9a and 9c (Wang et al. 2004; Chen et al. 2012), while the local
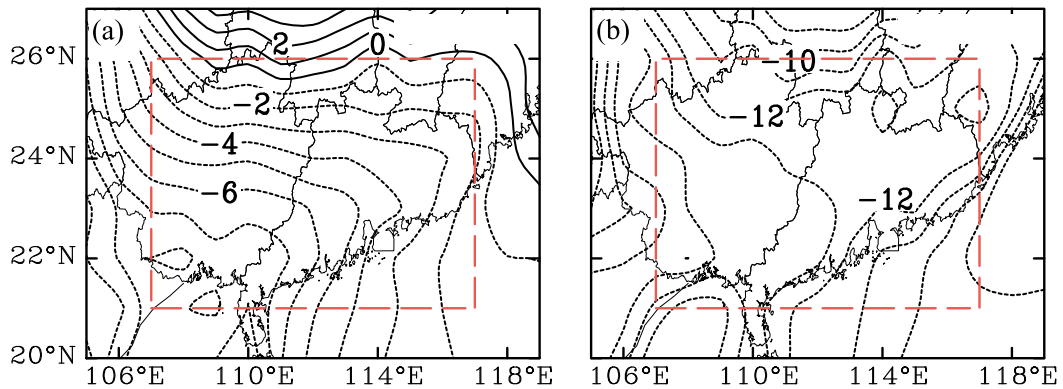

FIG. 15. The equivalent potential temperature difference between 500 and 850 hPa at 1400 BST during the (a) premonsoon-onset period and (b) postmonsoon-onset period.

thermodynamic instability can be detected from θ_e difference between 500 and 850 hPa at 1400 BST (Fig. 15). It seems that the lower troposphere during the premonsoon onset is more stable than that during the postmonsoon-onset period. Weak stability during the postmonsoon-onset period is more favorable for the occurrence of the afternoon rainfall. Therefore, the afternoon rainfall is more active during the postmonsoon-onset period, which is consistent with Luo et al. (2013), who noted the MCSs were less controlled by large-scale pressure systems but more by local instability associated with surface heating during the postmonsoon and monsoon-break periods.

5. Summary and discussion

In this study, we examine the diurnal variations of the presummer rainfall over southern China, focusing mainly on the regions of Guangxi and Guangdong Provinces, using the merged gauge-satellite high-resolution gridded hourly rainfall dataset during April–June of 2008–15. Results show large diurnal variations in rainfall amount, frequency, and intensity, different diurnal rainfall production modes across southern China and different diurnal rainfall characteristics between the pre- and postmonsoon-onset periods. Main findings are summarized as follows:

- There are two diurnal rainfall peaks in southern China, with one occurring in the early morning hours and the other in the late afternoon. The early morning rainfall amount and frequency peaks are both higher than those in the afternoon during the premonsoon-onset period, whereas the two rainfall peaks are almost equal in amplitude during the postmonsoon-onset period with higher rainfall intensity in the morning and higher rainfall frequency in the afternoon.
- The peak rainfall in southwestern China appears in the early morning, most of which is associated with the development of a nocturnal low-level southwesterly wind, through the supply of tropical high-θ_e air, whereas the peak rainfall in southeastern China occurs in the late afternoon, most of which is generated due to surface heating. Land–sea breezes also contribute to the afternoon rainfall in southeastern China especially during the post monsoon-onset period.
- There are three propagating DCR modes accounting for the total presummer rainfall over southern China: an eastward- or southeastward-propagating mode (mostly over southwestern China), a quasi-stationary mode, and an inland-propagating mode associated with land–sea breezes both over southeastern China.

It should be mentioned that due to the lack of high-resolution data, an accurate description of the diurnal cycle and the associated dynamical and thermodynamical processes is not possible. In particular, the NCEP's FNL analysis, though representing well large-scale conditions, still departs from what happens in nature, especially at the mesoscale and convective scale. In this context, numerical simulations of some representative cases could be performed to gain insight into the roles of various processes, such as orography, cloud–radiation interaction, sea–land contrast, and convective downdrafts, in determining the DCR of southern China during the pre- and postmonsoon-onset periods.

REFERENCES

Bao, X. H., F. Q. Zhang, and J. H. Sun, 2011: Diurnal variations of warm-season precipitation east of the Tibetan Plateau over China. *Mon. Wea. Rev.*, **139**, 2790–2810, doi:10.1175/MWR-D-11-00006.1.

Chen, G. X., W. M. Sha, and T. Iwasaki, 2009: Diurnal variation of precipitation over southeastern China: Spatial distribution and its seasonality. *J. Geophys. Res.*, **114**, D13103, doi:10.1029/2008JD011103.

——, W. Sha, T. Iwasaki, and K. Ueno, 2012: Diurnal variation of rainfall in the Yangtze River Valley during the spring-summer transition from TRMM measurements. *J. Geophys. Res.*, **117**, D06106, doi:10.1029/2011JD017056.

Chen, H. M., T. J. Zhou, R. C. Yu, and J. Li, 2009: Summer rain fall duration and its diurnal cycle over the U.S. Great Plains. *Int. J. Climatol.*, **29**, 1515–1519, doi:10.1002/joc.1806.

——, R. C. Yu, J. Li, W. H. Yuan, and T. J. Zhou, 2010: Why nocturnal long-duration rainfall presents an eastward delayed diurnal phase along the Yangtze River. *J. Climate*, **23**, 905–917, doi:10.1175/2009JCLI3187.1.

Chen, J., Y. G. Zheng, X. L. Zhang, and P. J. Zhu, 2013: Distribution and diurnal variation of warm-season short-duration heavy rainfall in relation to the MCSs in China. *Acta Meteor. Sin.*, **27**, 868–888, doi:10.1007/s13351-013-0605-x.

Chen, X. C., K. Zhao, and M. Xue, 2014: Spatial and temporal characteristics of warm season convection over Pearl River Delta region, China, based on 3 years of operational radar data. *J. Geophys. Res. Atmos.*, **119**, 12 447–12 465, doi:10.1002/2014JD021965.

——, ——, ——, B. Zhou, X. Huang, and W. Xu, 2015: Radar-observed diurnal cycle and propagation of convection over the Pearl River Delta during Mei-Yu season. *J. Geophys. Res. Atmos.*, **120**, 12 557–12 575, doi:10.1002/2015JD023872.

Dai, A. G., F. Giorgi, and K. E. Trenberth, 1999: Observed and model simulated precipitation diurnal cycle over the contiguous United States. *J. Geophys. Res.*, **104**, 6377–6402, doi:10.1029/98JD02720.

Ding, Y. L., 1992: Summer monsoon rainfalls in China. *J. Meteor. Soc. Japan*, **70**, 373–396.

——, 1994: *Monsoons over China*. Kluwer Academy, 419 pp.

——, and J. C. L. Chan, 2005: The East Asian summer monsoon: An overview. *Meteor. Atmos. Phys.*, **89**, 117–142, doi:10.1007/s00703-005-0125-z.

Huang, S. S., 1986: *The Heavy Rain during the Pre-summer Period over Southern China* (in Chinese). Guangdong Technology Press, 244 pp.

Joyce, R. J., J. E. Janowiak, P. A. Arkin, and P. Xie, 2004: CMORPH: A method that produces global precipitation estimates from passive microwave and infrared data at high spatial and temporal resolution. *J. Hydrometeor.*, **5**, 487–503, doi:10.1175/1525-7541(2004)005<0487:CAMTPG>2.0.CO;2.

Kincer, J. B., 1916: Daytime and nighttime precipitation and their economic significance. *Mon. Wea. Rev.*, **44**, 628–633, doi:10.1175/1520-0493(1916)44<628:DANPAT>2.0.CO;2.

Landin, M. G., and L. F. Bosart, 1985: Diurnal variability of precipitation in the northeastern United States. *Mon. Wea. Rev.*, **113**, 989–1014, doi:10.1175/1520-0493(1985)113<0989:DVOPIT>2.0.CO;2.

Li, B., L. P. Liu, S. X. Zhao, and C. Y. Huang, 2013: Numerical experiment of the effect of local low terrain on heavy rainstorm of South China (in Chinese with English abstract). *Plateau Meteor.*, **32** (6), 1638–1650.

Li, J., R. C. Yu, and T. J. Zhou, 2008: Seasonal variation of the diurnal cycle of rainfall in southern contiguous China. *J. Climate*, **21**, 6036–6043, doi:10.1175/2008JCLI2188.1.

Liang, X. Z., L. Li, A. G. Dai, and K. E. Kunkel, 2004: Regional climate model simulation of summer precipitation diurnal cycle over the United States. *Geophys. Res. Lett.*, **31**, L24208, doi:10.1029/2004GL021054.

Luo, Y. L., 2016: Advances in understanding the early-summer heavy rainfall over south China. *The Global Monsoon System, III: A WMO Quadrennial Review*, C.-P. Chang et al., Eds., World Scientific Series on Asia-Pacific Weather and Climate, Vol. 9, World Scientific, in press.

——, H. Wang, R. H. Zhang, W. Qian, and Z. Luo, 2013: Comparison of rainfall characteristics and convective properties of monsoon precipitation systems over South China and the Yangze and Huai River Basin. *J. Climate*, **26**, 110–132, doi:10.1175/JCLI-D-12-00100.1.

——, Y. Gong, and D. L. Zhang, 2014: Initiation and organizational modes of an extreme-rain-producing mesoscale convective system along a mei-yu front in east China. *Mon. Wea. Rev.*, **142**, 203–221, doi:10.1175/MWR-D-13-00111.1.

Nozumi, Y., and H. Arakawa, 1968: Prefrontal rain bands located in the warm sector of subtropical cyclones over the ocean. *J. Geophys. Res.*, **73**, 487–492, doi:10.1029/JB073i002p00487.

Pan, Y., Y. Shen, Q. Q. Yu, and P. Zhao, 2012: Merged analyses of gauge-satellite hourly precipitation over China based on OI technique (in Chinese with English abstract). *Acta Meteor. Sin.*, **70**, 1381–1389.

Sun, J. H., and S. X. Zhao, 2002: A study of mesoscale convective systems and its environmental fields during the June 1994 record heavy rainfall in South China. Part II: Effect of physical processes, initial environmental fields and topography on meso-β convective system (in Chinese). *Chin. J. Atmos. Sci.*, **26**, 633–646.

Tao, S. Y., 1981: *Storm Rainfall in China* (in Chinese). Science Press, 225 pp.

——, and L. X. Chen, 1987: A review of recent research on the East Asian summer monsoon in China. *Monsoon Meteorology*, T. N. Krishnamurti and C. P. Chang, Eds., Oxford University Press, 60–92.

Wallace, J. M., 1975: Diurnal variations in precipitation and thunderstorm frequency over the conterminous United States. *Mon. Wea. Rev.*, **103**, 406–419, doi:10.1175/1520-0493(1975)103<0406:DVIPAT>2.0.CO;2.

Wang, C. C., G. T. Chen, and R. E. Carbone, 2004: A climatology of warm-season cloud patterns over East Asia based on GMS infrared brightness temperature observations. *Mon. Wea. Rev.*, **132**, 1606–1629, doi:10.1175/1520-0493(2004)132<1606:ACOWCP>2.0.CO;2.

Xu, W. X., and E. J. Zipser, 2011: Diurnal variations of precipitation, deep convection, and lightning over and east of the eastern Tibetan Plateau. *J. Climate*, **24**, 448–465, doi:10.1175/2010JCLI3719.1.

——, ——, and C. Liu, 2009: Rainfall characteristics and convective properties of mei-yu precipitation systems over South China, Taiwan, and the South China Sea. Part I: TRMM observations. *Mon. Wea. Rev.*, **137**, 4261–4275, doi:10.1175/2009MWR2982.1.

Yamada, T. J., M. I. Lee, M. Kanamitsu, and H. Kanamaru, 2012: Diurnal characteristics of rainfall over the contiguous United States and northern Mexico in the dynamically downscaled reanalysis dataset (US10). *J. Hydrometeor.*, **13**, 1142–1148, doi:10.1175/JHM-D-11-0121.1.

Yu, R. C., T. J. Zhou, A. Y. Xiong, Y. Zhu, and J. Li, 2007: Diurnal variations of summer precipitation over contiguous China. *Geophys. Res. Lett.*, **34**, L01704, doi:10.1029/2006GL028129.

Zhang, D.-L., 1998: Roles of various diabatic physical processes in mesoscale models (in Chinese). *Chin. J. Atmos. Sci.*, **22**, 548–561.

——, and J. M. Fritsch, 1986: Numerical simulation of the meso-β scale structure and evolution of the 1977 Johnstown Flood. Part I: Model description and verification. *J. Atmos. Sci.*, **43**, 1913–1943, doi:10.1175/1520-0469(1986)043<1913:NSOTMS>2.0.CO;2.

——, and ——, 1988: Numerical sensitivity experiments of varying model physics on the structure, evolution, and dynamics of two mesoscale convective systems. *J. Atmos. Sci.*, **45**, 261–293, doi:10.1175/1520-0469(1988)045<0261:NSEOVM>2.0.CO;2.

Zheng, Y. G., and J. Chen, 2011: A climatology of deep convection over south China and adjacent seas during summer. *J. Trop. Meteor.*, **27**, 495–508.

Zhou, T. J., R. C. Yu, H. M. Chen, A. Dai, and Y. Pan, 2008: Summer precipitation frequency, intensity, and diurnal cycle over China: A comparison of satellite data with rain gauge observations. *J. Climate*, **21**, 3997–4010, doi:10.1175/2008JCLI2028.1.